AIAA 80-1371R

Temperature Profile Measurements Using CO Line Absorption at Different Vibrational Levels

W. Cheng* and F. Bien†
Aerodyne Research, Inc., Bedford, Mass.

The temperature profile of a laboratory methane/coal burner is measured by taking the ratio of absorptions for a pair of CO vibration-rotation lines with a tunable diode laser system. Assuming an axisymmetric temperature profile, a scan of the cross section of the burner provides an absorption profile which can be inverted into a radial temperature profile by Abel transformation. By selecting the vibrational levels of the CO absorption lines, different optical depths can be achieved by probing the flame. The feasibility of temperature profile measurement is demonstrated by measuring the temperature of a methane/coal burner using a second derivative system on the P_0 (32) and the P_2 (21) CO absorption lines.

Introduction

THE gas temperature and temperature profile are important parameters in determining the performance of a combustor. Measurements of these parameters using thermocouples have the problem of thermocouple survival in high temperature oxidizing flames. Point measurements using optical techniques such as coherent anti-Stokes Raman spectroscopy[1] require large optical access not often available in such furnaces. We use a line-of-sight optical technique and Abel inversion to obtain the temperature profile in a laboratory methane/coal burner.

The standard technique for the determination of flame temperature is to use sodium or potassium line reversal.[2-4] When the optical depth becomes large, however, measurements become difficult because of the self-absorption in cold boundary layers. Line-of-sight measurements of temperature using CO vibrational line absorption[5,6] has the advantage over line reversal techniques in that nonoptically black absorption lines can be chosen by selecting different vibrational transitions of CO. An additional advantage in using the CO absorption of radiation from a tunable diode laser is that this system can be used through a limited optical access by collimating the laser radiation.

We have measured gas temperature using the CO absorption technique in the wing of the $v=0$ vibrational band and near the maximum of the $v=2$ vibrational band in the presence of a cool boundary layer in an axisymmetric methane/coal burner. By making an Abel transformation on line-of-sight measurements across the flame, the temperature profile is obtained. In the following sections, we discuss the temperature sensitivity to vibration levels and present measurements made in our laboratory methane/coal burner together with thermocouple measurements for comparison.

Theory of Measurement

The technique of measuring temperature using the ratio of CO line absorption from two vibration-rotation levels has been previously discussed.[6] The two lines are typically chosen within 1 cm^{-1} from each other so that they can be scanned by the same mode of a tunable laser diode. For a homogeneous medium in thermal equilibrium, the ratio of the transmittance at the line center of the two neighboring lines, assuming that there is no line interference, is

$$\frac{[\ell n(I/I_0)]_2}{[\ell n(I/I_0)]_1} = \frac{S_2(T)}{S_1(T)} \tag{1}$$

where the ratio of the temperature dependent line strengths S_2/S_1, is given by[7]

$$\frac{S_2}{S_1} = \frac{\{(v+1)G(J)(N_{vJ}/N)/(2J+1)\}_2}{\{(v+1)G(J)(N_{vJ}/N)/(2J+1)\}_1} \tag{2}$$

Here (v, J) are the lower state quantum numbers, $G(J)=J$ for a P branch transition and $J+1$ for an R branch transition, and N_{vJ}/N is the fractional Boltzmann distribution at temperature T. Therefore the temperature can be calculated from the ratio of the measured transmittance.

The temperature dependence of S_2/S_1 is contained in the Boltzmann factor $N_{v,J}/N$, for which the temperature sensitivity is given, to first order in v and J, by

$$\frac{d\ell n(N_{v,J}/N)}{d\ell n(T)} = -1+J(J+1)\frac{hcB_v}{k_T}+\frac{hc\omega_v}{kT} \times\left[v-\frac{\exp(-hc\omega_v/kT)}{1-\exp(-hc\omega_v/kT)}\right] \tag{3}$$

This expression is a monotonically increasing function of both v and J, with a much larger dependence on v than on J. Contour plots of the temperature sensitivity Eq.(3) as a function of v and J values at 2000 K are shown in Fig. 1. High temperature sensitivity can be obtained by ratioing a high v, J line to a low v, J line. In practice, however, the absorption for the high v, J lines is very low, and tradeoffs must be made between high temperature sensitivity and measurement accuracy.

Since the temperature sensitivity is much more sensitive to the vibrational level than to the J level of the CO lines, it is instructive to study the temperature dependence of the temperature sensitivity for various v by arbitrarily fixing $J=2$. Such a dependence is shown in Fig. 2. The temperature sensitivity increases with increase in v and decreases with increase in temperature. Fortunately, as the temperature increases, more high v states are populated and the absorption, hence the signal-to-noise ratio of the absorption measurement for the high v lines, increases with increase in

Presented as Paper 80-1371 at the AIAA 13th Fluid and Plasma Dynamics Conference, Snowmass, Colo., July 14-16, 1980; submitted Sept. 18, 1980; revision received Feb. 20, 1981.

*Senior Research Scientist; also, Assistant Professor of Mechanical Engineering, Massachusetts Institute of Technology. Member AIAA.

†Principal Research Scientist; present address: Spectral Science, Inc., Burlington, Mass.

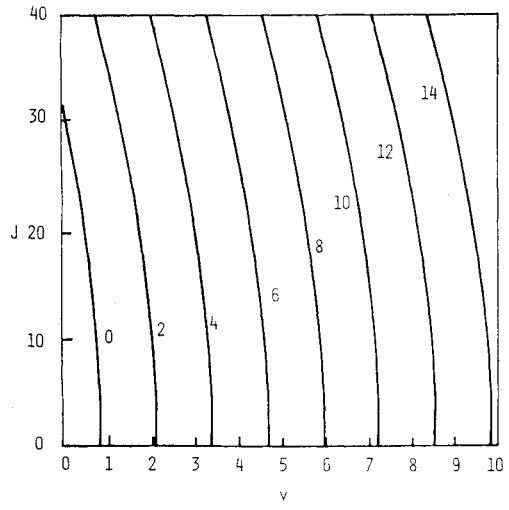

Fig. 1 Temperature sensitivity ($d\ell n(N_{v,J}/N)/d\ell n\ T$) contours for various v, J, CO lines at 2000 K.

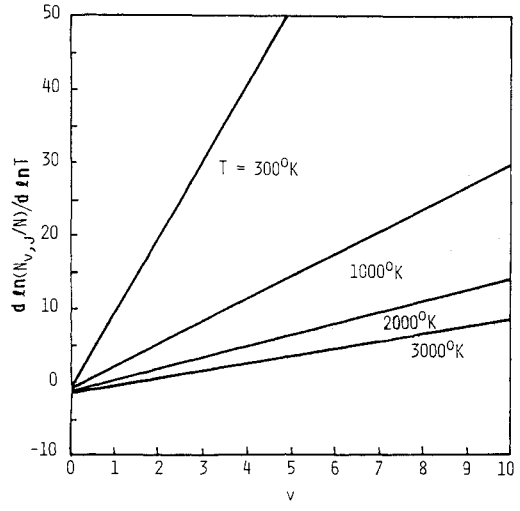

Fig. 2 Temperature sensitivity at various temperatures for different v lines, $J=2$.

temperature. Therefore, optimal temperature sensitivity can be achieved by going to the highest v line with acceptable measurement accuracy.

We have developed a system using second-derivative spectroscopy for our temperature measurement. Such a system, which suppresses the base line, can offer substantial improvement in accuracy over direct absorption measurements. It is straightforward to show that the second-derivative signal at the line center of a pressure broadened line is given by[8]

$$\frac{d^2I}{d\omega^2}\bigg|_{\omega_l} = \left(\frac{S_l \chi p}{\pi}\frac{2}{b_l^3}\right)\ell I(\omega_l) \tag{4}$$

where S_l is the line strength, χ the mole fraction of CO, p the pressure, b_l the line collisional half width, and ℓ the absorption path length. This pressure-broadened profile is applicable for high pressure flames at moderate temperatures. For low pressure flames at high temperatures, the Doppler broadening becomes significant and a Voight profile is appropriate. It is shown in the Appendix that Doppler broadening becomes important when the Voight parameter is below 3. For an atmospheric flame, the corresponding temperature is approximately 1500 K. Applying Eq. (4) to the two lines, we obtain

$$\left(\frac{1}{I}\frac{d^2I}{d\omega^2}\right)_{\omega_2} \Big/ \left(\frac{1}{I}\frac{d^2I}{d\omega^2}\right)_{\omega_1} = \left(\frac{S_2}{S_1}\right)\left(\frac{b_1}{b_2}\right)^3 \tag{5}$$

Measurements and theoretical considerations[9] have indicated that the collision half width b varies as $T^{0.75}$ and is insensitive to J, therefore the ratio b_1/b_2 is only a function of J. The values of b as a function of J have been reported in several papers[10-12]; b generally decreases with increasing J, and, depending on the J values, can vary by 10-20%. Therefore, it is important to include the ratio b_1/b_2 in solving Eq. (5) for the temperature. In our measurement, we have used the b values of Ref. 10, which is based on measurement of CO line width in flames. Therefore, all the information for determination of temperature from Eq. (5) is available.

Similar to Eq. (1), Eq. (5) involves measurements of ratios and, therefore, is self-calibrating if the measurements are made simultaneously. However, unlike Eq. (1), where the incident intensity $I_0(\omega)$ is required in the intensity ratio, Eq. (5) involves the transmitted intensity $I(\omega)$. The need for a reference beam measurement is thus eliminated. Line interference effects are minimized since the second-derivative at the tail of the interfering line is usually small at the absorbing line. Similarly, the broad band effects of absorption and scattering due to presence of particulates is also minimized.[13] A lower limit of detectable absorption of 2×10^{-5} in a quiescent environment has been reported.[14] For absorption measurements in practical burner environments, the S/N is degraded by refractive index variations of the hot gas, turbulent temperature and CO concentration fluctuations of the flame, and the mechanical vibration of the optical components.

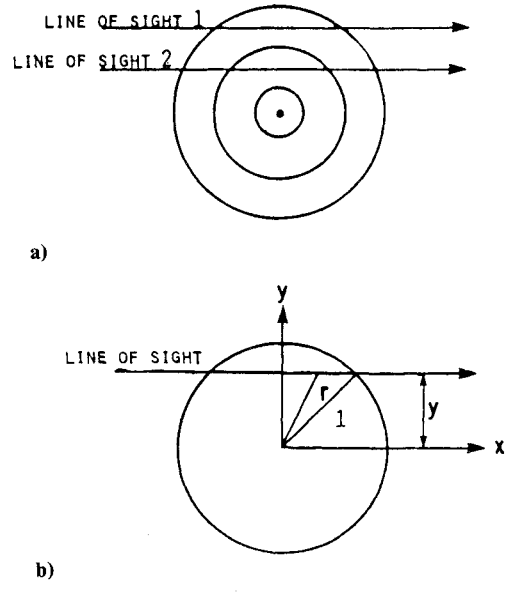

Fig. 3 a) Illustration of the principle of Abel inversion; b) geometry of Abel inversion.

Temperature Profile Measurement

For a nonhomogeneous medium, Eq. (4) may be generalized as

$$\frac{d^2I}{d\omega^2}\bigg|_{\omega_l} = I(\omega_l)\int \frac{S_l \chi p}{\pi}\frac{2}{b_l^3}dx \tag{6}$$

where the integration is evaluated along the line-of-sight. The measurement is, therefore, a convolution of the line strength and the line width profiles with the CO concentration profile for a given pressure p. A line-of-sight temperature may be calculated by direct application of Eq. (5), but the actual

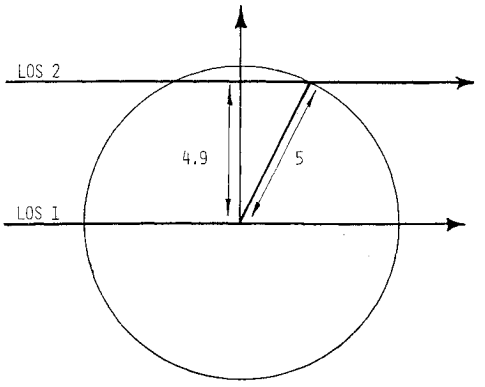

Fig. 4 Line-of-sight positions.

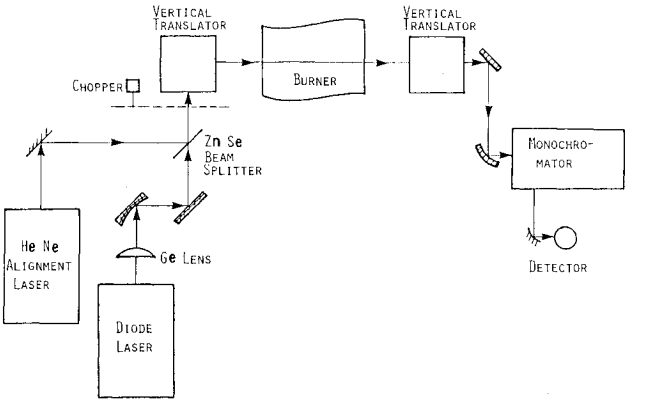

Fig. 5 CO line absorption temperature measurement optical schematic.

temperature can only be obtained by deconvoluting measurements at different line-of-sight positions.

A particularly simple, yet often encountered situation is an axisymmetric medium such as the hot gas in a cylindrical burner. In this case, (Fig. 3a), line-of-sight measurement at one position can be subtracted from a measurement at an adjacent position to yield information on the property of the medium at the differential optical path. This is formally expressed by the Abel transform which inverts the line-of-sight measurements $g(y)$ to the radial profile $f(r)$. Referring to Fig. 3b, the line-of-sight measurement is

$$g(y) = 2\int_0^{\sqrt{1-y^2}} f[r(x,y)]\,dx \tag{7}$$

and the radial profile is then

$$f(r) = \frac{1}{\pi}\int_r^1 \frac{dg}{dy}\frac{dy}{\sqrt{y^2-r^2}} \tag{8}$$

In the above equations, all lengths are normalized with respect to the radius of the burner. Applying Eq. (8) to Eq. (6), the values of $S\chi p/b^3$ for the two lines as a function of radius can be obtained. By ratioing the values obtained for each line, S_2/S_1, and therefore the temperature can be obtained for each radial position. The details of the inversion process are presented in the Appendix.

Selection of CO Absorption Lines

In applying the CO absorption line temperature measurement technique to large burners, the absorption for the low vibrational (v) rotational (J) lines at line-of-sight through the center of the burner are often black which renders accurate measurement difficult. This difficulty can be avoided either by using the absorption lines of the CO isotopes ($^{13}C^{16}O$ is 1.11% abundant and $^{12}C^{18}O$ is 0.2% abundant), or by using the higher v, J lines. Since the temperature measurement is most sensitive when the absorption from a high v, J line is ratioed to that of a low v, J line, the optimal line selection is therefore a high v, J absorption line of $^{12}C^{16}O$ combined with a low v, J absorption line of one of the isotopes.

Where the line-of-sight is close to the edge of the burner, however, there is little absorption for the high v, J lines because of the lower temperature. Therefore, to measure temperature profiles accurately, it is necessary to use more than one pair of v, J lines. To illustrate this concept, consider a 5 m radius burner (Fig. 4). Assume the line-of-sight temperature is 2000 K in position 1 and 1000 K in position 2. Also assume that there is 1% CO. If we use the line pair $P_4(9)$ of $^{12}C^{16}O$ (at 2003.17 cm^{-1}) and P_0 (23) of $^{13}C^{16}O$ (at 2003.52 cm^{-1}) the absorptions at position 1 are 42 and 47%. These are easily measurable numbers. However, the absorptions at position 2 become 0.08 and 20%, respectively. Accurate measurement of the $P_4(9)$ line may be difficult. Alternatively, consider the line pair $P_0(16)$ of $^{13}C^{16}O$ (at 2033.42 cm^{-1}) and $P_1(2)$ of $^{12}C^{16}O$ (at 2034.15 cm^{-1}). The absorptions at position 2 are 5 and 83%, which are easily measurable. However, the absorptions at position 1 are 4 and ~100%. The latter is optically black and not readily measurable. It is therefore necessary to use both line pairs for accurate temperature profile measurement.

The additional constraint in selecting CO line pairs is that there are no interfering absorption lines from other molecules along the line-of-sight. Because of the very strong radiances from $CO_2(\nu_3)$ centered at 4.3 μm, and $H_2O(\nu_1, \nu_3)$ at 6.3 μm, the measurement is limited to a region just below 5 μm.

Experimental Configuration

Temperature profile measurements have been performed on a methane/coal burner.[15] The burner has an inside diameter of 12.25 cm and is 75 cm long. The burner wall is made of zirconia which is a good insulator and can withstand temperatures up to 2300 K. The burner has two flame zones. An inner core where pulverized coal is burnt with premixed methane and oxygen enriched air and an outer guard flame of premixed methane and oxygen enriched air.

The optical setup is shown in Fig. 5. Optical access to the burner is provided by two 12.25 × 0.3 cm slits located 55 cm downstream of the burner. Radiation heat loss by the flame through the slit is minimal. The light source is provided by a cryogenically cooled laser diode from Laser Analytics, Inc. Wavelength tuning can be achieved by varying the temperature of the diode or the diode current. Referring to Fig. 5, the laser radiation is focused into a 2 mm diam beam by a germanium lens and a toroidal mirror. The beam is steered through the optical access of the burner into the monochromator/detector system by a pair of vertical translators so that the cross section of the burner can be scanned. The diode laser usually lases in several modes separated by 0.5 to 1 cm^{-1} in the region around 2000 cm^{-1}. This wavelength region was selected as it fell between the strong $CO_2(\nu_3)$ and water bands. The monochromator selects the single mode whose wavelength is current tunable through the absorption line. In addition, the monochromator rejects much of the blackbody radiation from the burner to improve signal-to-noise ratio.

The second-derivative signal and the transmission signal are measured simultaneously using the same detector. The laser line is current tuned with a small wavelength modulation at 1 kHz while at the same time a slow current ramp is applied which tunes the wavelength over the absorption lines. The slow tuning rate is approximately 0.01 cm^{-1}/s. In addition, a mechanical chopper is also used. Two lock-in amplifiers are used so that by locking one to the chopping frequency and locking the other to twice the modulation frequency, the

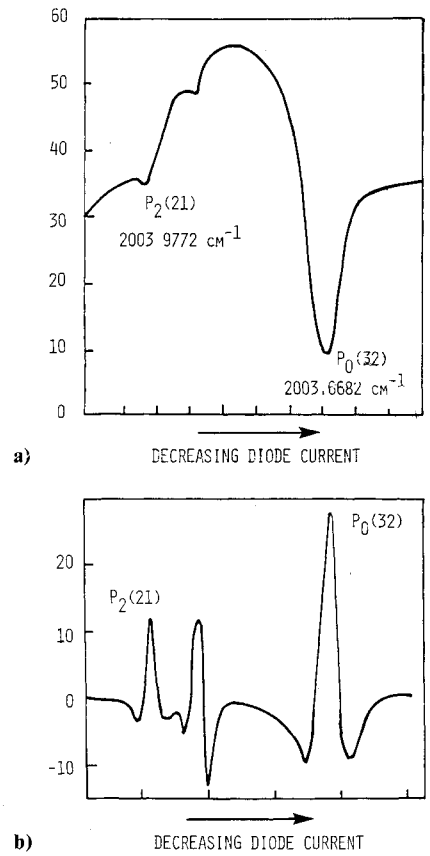

Fig. 6 a) Transmission spectrum of the $P_0(32)$ and $P_2(21)$ lines of CO. Horizontal axis is laser diode current. The structure between the two lines is due to diode laser anomaly. b) Corresponding second derivative spectrum.

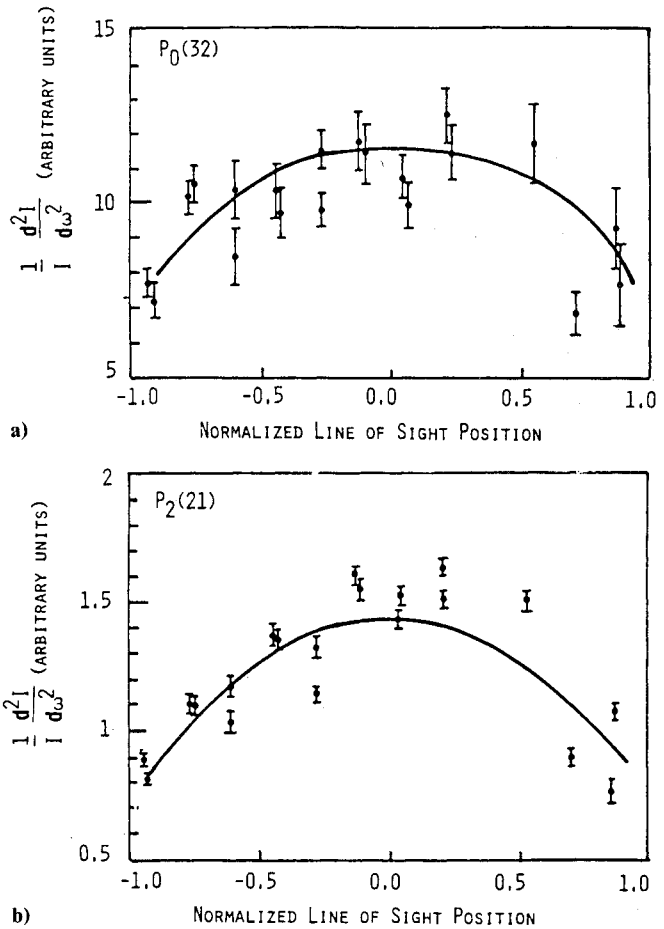

Fig. 7 a) Normalized second-derivative data, $P_0(32)$ CO absorption line. Line-of-sight position is normalized with respect to burner radius; b) data for $P_2(21)$ CO absorption line. Solid line is polynomial fit to the data.

transmission and the second-derivative signals are obtained simultaneously from the output of respective amplifiers. By finding the ratio of the second-derivative signal to the transmission signal, the above arrangement has calibrated out the laser intensity variation, monochromator slit function, detector drift and optical misalignments. Then, finding the ratio of the results of the pair of absorption lines, the gain transfer functions of the second-derivative system and the transmission system is calibrated out, making the method self-calibrating.

In the current configuration, approximately 1 min is used to obtain a spectral scan at each line-of-sight location. The total elapsed time for scanning the burner cross section is approximately 30 min. The data include scanning the spectrum twice (with increasing and decreasing diode current tuning) at each of the 11 spatial locations. It should be noted that most of the time is spent in scanning the wavelength of the diode laser from one absorption line to the other. In principle, a system can be designed to scan the laser output wavelength across one absorption line and then jump immediately to scan across the next line. It is estimated that then 10 s of measurement time is needed for each line-of-sight location. Allowing 10 s for beam translation operation, the complete scanning of the burner cross section would take approximately 3.5 min.

Experimental Results

We have measured the temperature profile of the burner operating at a fuel rich condition (stoichiometric ratio = 1.12). The overall gas flow rate is 100 g/min and the pulverized coal flow rate is 2 g/min. Luminous particles from incomplete combustion of coal are sometimes visible through the optical access slits but they do not seem to interfere with the temperature measurement.

The CO absorption lines used for the temperature profile measurements are the $P_0(32)$ and $P_2(21)$ lines of $^{12}C^{16}O$. A typical transmission spectrum and second-derivative spectrum is shown in Fig. 6. The disruptive signal between the two absorption lines in the second-derivative spectrum is due to an anomaly of the diode laser. It is evident from the transmission spectrum that there is great uncertainty in assigning I_0 at the absorption peak, hence a measurement of transmission is difficult. However, measurement of I from the transmission spectrum and $d^2I/d\omega^2$ from the second-derivative spectrum can be done easily. This comparison illustrates the advantages of the second-derivative method over the direct transmission measurement.

In Fig. 7, the second-derivative signal normalized by the transmitted signals for the two absorption lines are plotted as a function of the line-of-sight positions. A fourth degree polynomial, forced to be symmetric about the centerline, is fit to the data. These line-of-sight profiles are then inverted by the Abel transform (see Appendix) to obtain the radial temperature profile. The scatter in the data was attributed to variations in CO concentration with time. This was borne out by the correlation between measurements of the two vibrational levels with each other when the two measurements were taken at the same time.

The radial temperature profile is obtained through the Abel inverted second-derivative signal profile using Eq. (A10) of the Appendix. The inverted temperature profile is plotted in Fig. 8 together with the temperature profile obtained from traversing thermocouple measurements in two orthogonal directions for comparison. In addition, the line-of-sight temperature obtained from direct application of Eq. (5)

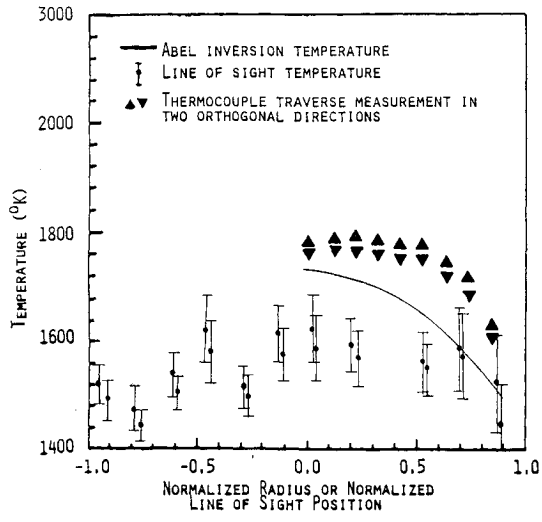

Fig. 8 Abel inversion temperature profile, thermocouple measured temperature profile, and line-of-sight temperature profile.

without inversion is also plotted. In general, the line-of-sight temperature is different from the true temperature because it is a convoluted average of the temperature profile.

It is difficult to assign exact error estimates to the inverted temperature profile because of the Abel transformation. A reasonable assumption is that the temperature error is of the same order as the line-of-sight temperature error estimate. The inverted temperature is approximately 7% lower than the thermocouple measured temperature. This is within the measurement error of the experiment.

Conclusions

We have studied the technique of measuring the flame temperature by ratioing the line strengths of a pair of vibrational lines of CO. By taking the ratios of the second-derivative of the absorption with respect to the laser wavelength for two lines as well as the ratios of their transmittances, a self-calibrating temperature measurement technique has been devised. We have determined the temperature profile of an axisymmetric methane/coal burner by taking line-of-sight measurements into a radial profile using the Abel transformation. The temperature profile obtained from a fit to the data from the $P_0(32)$ and $P_2(21)$ lines shows some scatter which can be attributed to temporal variation of CO concentration.

In applying this method to large, power plant scale burner, it would be necessary to use more than one line pair for making an accurate temperature profile measurement. This is because of the difference in optical depths of the absorption lines comparing a line-of-sight through the hot burner core to a line-of-sight through the cooler boundary layer.

Appendix

Case When Doppler Broadening is Significant

For moderate pressure flame at high temperatures, both collision and Doppler broadening are significant, and a Voight line profile has to be used in place of the Lorentzian profile. Therefore Eqs. (4) and (5) have to be modified appropriately. For an arbitrary line shape function $\phi(\omega-\omega_0)$, the ratio of the second-derivative signals of two lines may be expressed as

$$\left(\frac{1}{I}\frac{\mathrm{d}^2 I}{\mathrm{d}\omega^2}\right)_2 \Big/ \left(\frac{1}{I}\frac{\mathrm{d}^2 I}{\mathrm{d}\omega^2}\right)_1 = \frac{S_2}{S_1}\left[\left(\frac{\mathrm{d}^2\phi}{\mathrm{d}\omega^2}\right)_2 \Big/ \left(\frac{\mathrm{d}^2\phi}{\mathrm{d}\omega^2}\right)_1\right] \tag{A1}$$

where the line shape derivatives are to be evaluated at the line center ω_0 of the respective lines. For a Voight profile, the line shape function ϕ is

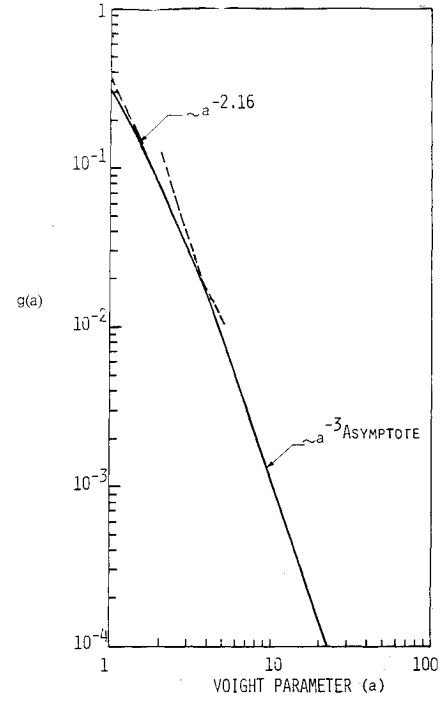

Fig. A1 Second-derivative function of Voight profile at line center as function of a.

$$\phi_v \equiv \frac{1}{b_D}\sqrt{\frac{\ell n 2}{\pi}}\,\frac{a}{\pi}\int_{-\infty}^{\infty}\frac{e^{-y^2}\mathrm{d}y}{a^2+(x-y)^2} \tag{A2}$$

where

$$x \equiv (\omega-\omega_0)\sqrt{\ell n 2}/b_D \tag{A3}$$

and b_D is the Dopper half width. The Voight parameter a is a measure of the relative importance of collision and Doppler broadening

$$a \equiv \sqrt{\ell n 2}\; b_c/b_D \tag{A4}$$

If the collision half width b_c is large compared with b_D, the Voight profile approaches a Lorentzian profile

$$\phi_L = \frac{1}{b_D}\sqrt{\frac{\ell n 2}{\pi}}\,\frac{a}{\sqrt{\pi}}\,\frac{1}{a^2+x^2} \tag{A5}$$

The second-derivatives at the line center of the Lorentzian and the Voight profiles are

$$\frac{\mathrm{d}^2\phi_L}{\mathrm{d}\omega^2} = \frac{1}{b_D^3}\,\frac{(\ell n 2)^{3/2}}{\sqrt{\pi}}\left[\frac{-2}{\sqrt{\pi}a^3}\right] \tag{A6}$$

$$\frac{\mathrm{d}^2\phi_v}{\mathrm{d}\omega^2} = \frac{1}{b_D^3}\,\frac{(\ell n 2)^{3/2}}{\sqrt{\pi}}\,[-g(a)] \tag{A7}$$

where

$$g(a) \equiv \frac{4a}{\pi}\int_0^{\infty}\frac{\mathrm{d}y e^{-y^2}}{(a^2+y^2)^2}\left(1-\frac{4y^2}{a^2+y^2}\right) \tag{A8}$$

It can be readily shown that the expression in Eq. (A7) approaches that in Eq. (A6) for large a.

Equation (A8) has been integrated numerically and the result is shown in Fig. A1. For a larger than 3, $g(a) \sim a^{-3}$ as in the Lorentzian profile. For $1.2 \le a \le 3$, $g(a)$ can reasonably be approximated as $g(a) \sim a^{-2.16}$. Therefore the corresponding expression in Eq. (A1) may be written as

$$\left(\frac{1}{I}\frac{d\,^2 I}{\mathrm{d}\omega^2}\right)_2 \Big/ \left(\frac{1}{I}\frac{\mathrm{d}^2 I}{\mathrm{d}\omega^2}\right)_1 = \frac{S_2}{S_1}\,\frac{(b_c^{-3})_2}{(b_c^{-3})_1} \quad \text{for } a>3 \tag{A9}$$

and

$$\left(\frac{1}{I}\frac{d^2I}{d\omega^2}\right)_2 \Big/ \left(\frac{1}{I}\frac{d^2I}{d\omega^2}\right)_1 = \frac{S_2}{S_1}\frac{(b_c^{-2.16})_2}{(b_c^{-2.16})_1}$$

for $1.2 \le a \le 3$ (A10)

Abel Inversion

Equation (8) involves the derivative of the measurement g, which in general, may be noisy. Therefore, it is necessary to do some filtering on g before Eq. (8) is used. Furthermore, for each value of r, Eq. (8) involves an integral from r to 1. Error can be substantial for r close to 1 because not may data points are available for numerical integration. Therefore, it is best to solve Eq. (8) exactly. This is possible if we fit a least square polynomial to the profile $g(y)$.

$$g(y) = a_0 + \sum_{i=2}^{N} a_i y^i$$

a_i is equal to zero because by symmetry dg/dy has to be zero at $y = 0$. Then

$$f(r) = \frac{1}{\pi}\sum_{i=2}^{N} a_i h_i(r) \qquad h_i(r) \equiv \int_r^1 \frac{y^{i-1}}{\sqrt{y^2 - r^2}}\,dy$$

The analytic results for $i = 2$ to 6 are

$$h_2(r) = \sqrt{1-r^2}$$

$$h_3(r) = -\frac{r^2}{2}\log r + \frac{1}{2}\sqrt{1-r^2} + \frac{r^2}{2}\log(1+\sqrt{1-r^2})$$

$$h_4(r) = \left[\frac{(1-r^2)^{3/2}}{3} + r^2\sqrt{1-r^2}\right]$$

$$h_5(r) = -\frac{3}{8}r^4\log r + \left(\frac{1}{4} + \frac{3}{8}r^2\right)\sqrt{1-r^2} + \frac{3}{8}r^4\log(1+\sqrt{1-r^2})$$

$$h_6(r) = \left[\frac{1}{5}(1-r^2)^{5/2} + \frac{2}{3}r^2(1-r^2)^{3/2} + r^4(1-r^2)^{1/2}\right]$$

Acknowledgment

This work has been performed under Contract No. EX-76-C-01-2478 to the Division of Magnetohydrodynamics, U. S. Department of Energy.

References

[1] Self, S. A. and Kruger, C. H., "Diagnostic Methods in Combustion MHD Flows," *Journal of Energy*, Vol. 1, Jan.-Feb. 1977, pp. 25-43.

[2] Daily, J. W. and Kruger, C. H., "Effects of Cold Boundary Layers on Spectroscopic Temperature Measurements in Combustion Gas Flows," *Journal of Quantitative Spectroscopy and Radiative Transfer*, Vol. 17, 1977, pp. 327-338.

[3] Yoshikawa, K. and Michiyoshi, I., "The Influence of Spatial Temperature Distribution and Measuring Configuration on Line-Reversal Temperature," *Journal of Quantitative Spectroscopy and Radiative Transfer*, Vol. 12, 1972, pp. 1673-1683.

[4] Thomas, D. L., "Problems in Applying the Line Reversal Method of Temperature Measurement to Flames," *Combustion and Flame*, Vol. 12, Dec. 1968, pp. 541-549.

[5] Hanson, R. K., Kuntz, P. A., and Kruger, C. H., "High Resolution Spectroscopy of Combustion Gases Using a Tunable IR Diode Laser," *Applied Optics*, Vol. 16, Aug. 1977, pp. 2045-2047.

[6] Hanson, R. K. and Falcone, P. K., "Temperature Measurement Technique for High Temperature Gases Using a Tunable Diode Laser," *Applied Optics*, Vol. 17, Aug. 1978, pp. 2477-2480.

[7] Penner, S. S., *Quantitative Spectroscopy and Gas Emissivities*, Addison Wesley, 1959, Chap. 7.

[8] Hinkley, E. D., Ku, R. T., and Kelley, P. L., "Techniques for Detection of Molecular Pollutants by Absorption of Laser Radiation," in *Topics in Applied Physics*, Vol. 14, *Laser Monitoring of the Atmosphere*, edited by E. D. Hinkley, Springer-Verlag, 1976, Chap. 26.

[9] Varanasi, P. and Sarangi, S., "Measurements of Intensities and Nitrogen-Broadened Linewidths in the CO Fundamental at Low Temperatures," *Journal of Quantitative Spectroscopy and Radiative Transfer*, Vol. 15, 1975, pp. 473-482.

[10] Dowling, J. A., Silverman, S., Benedict, W. S., and Quinn, J. W., "A Study of Line Shape of CO Infrared Emission Lines," *Journal of Research of the National Bureau of Standards, Section A: Physics and Chemistry*, Vol. 7JA, Sept.-Oct. 1971, pp. 469-477.

[11] Hunt, R. H., Toth, R. A., and Plyler, E. K., "High Resolution Determination of the Widths of Self-Broadened Lines of Carbon Monoxide, *Journal of Chemical Physics*, Vol. 49, Nov. 1968, pp. 3909-3912.

[12] Varghese, P. L. and Hanson, R. K., "Tunable Infrared Diode Laser Measurements of Line Strength and Collision Widths of $^{12}C^{16}O$ at Room Temperature," *Journal of Quantitative Spectroscopy and Radiative Transfer*, Vol. 24, 1980, pp. 479-489.

[13] Hanson, R. K., "Absorption Spectroscopy in Sooting Flames Using a Tunable Diode Laser," *Applied Optics*, Vol. 19, Feb. 1980, pp. 482-484.

[14] Reid, J., Shewchun, J., Garside, B. K., and Balik, E. A., "High Sensitivity Pollution Detection Employing Tunable Diode Lasers," *Applied Optics*, Vol. 17, No. 2, Jan. 1978, pp. 300-307.

[15] Yousefian, V., Wormhoudt, J., Kolb, C., Martinez Sanchez, M. and Kerrebrock, J., "Computer Modeling of Cool Ash Chemistry on the Performance of MHD Generators," *Proceedings of the 17th Symposium on Engineering Aspects of MHD*, Stanford, Calif., 1978.